RR-1282

DIODE-PUMPED Nd:YAG/Cr^{4+}:YAG MICROCHIP-LASER SYSTEM AT 214.8 nm FOR THE DETECTION OF NO

FINAL REPORT

J. WORMHOUDT*, J. H. SHORTER*, J. J. ZAYHOWSKI† AND C. COOK†

JULY 1999

U. S. ARMY RESEARCH OFFICE
4300 SOUTH MIAMI BOULEVARD
RESEARCH TRIANGLE PARK, NC 27709-2211

CONTRACT NUMBER
DAAG55-97-C-0001

*CENTER FOR MATERIALS RESEARCH
AERODYNE RESEARCH, INC.
BILLERICA, MA 01821
AND
†LINCOLN LABORATORY, MASSACHUSETTS INSTITUTE OF TECHNOLOGY
LEXINGTON, MA 02173-9108

TABLE OF CONTENTS

1. Introduction..... 1

2. Laser Development..... 2
   2.1 Operating Principle..... 2
   2.2 Optical Coating..... 3
   2.3 Device Operation..... 6

3. NO Fluorescence Observations..... 7
   3.1 Experimental Setup..... 7
   3.2 Spectral Position..... 8
   3.3 Spectral Model..... 9
   3.4 Comparison of Model and Observed Excitation Spectra..... 10
   3.5 Calibration and Detection Linearity..... 13
   3.6 Detection Sensitivity..... 13

4. SO_2 and NO_2 Observations with Microchip Lasers..... 15
   4.1 SO_2 Laser-Induced Fluorescence..... 15
   4.2 NO_2 Laser-Induced Fluorescence..... 15

5. Discussion and Conclusions..... 17

6. Acknowledgments..... 17

7. List of Publications and Technical Reports..... 18

8. List of All Participating Scientific Personnel..... 18

9. Report of Inventions..... 18

10. Bibliography..... 18

LIST OF ILLUSTRATIONS

Figure 1. Schematic of a 1.074-μm passively *Q*-switched microchip laser 2

Figure 2. Theoretical reflectivity of output coupler..... 4

Figure 3. Spectral runoff of optical coater with and without 6.5-cm distribution shield... 5

Figure 4. Spectral properties of output coatings on 12 microchip lasers (circles) and radially collocated witness samples (lines) 5

Figure 5. Photograph of optical head of fifth-harmonic 214.8-nm microchip laser source. 6

Figure 6. Schematic diagram of apparatus used in NO fluorescence observations..... 7

Figure 7. Filter bandpass curves (Oriel 51122 was used in experiments discussed here) and spectral locations and relative intensities of fluorescent emission lines (see Ref. 24) 8

Figure 8. Observed fluorescence excitation spectrum at 122 Torr (dots/dashes) and model prediction..... 11

Figure 9. Observed fluorescence excitation spectrum at 740 Torr (dashes) and model prediction..... 11

Figure 10. Observed fluorescence excitation spectrum at 240 Torr (dashes) and model prediction..... 12

Figure 11. Observed fluorescence excitation spectrum at 480 Torr (dashes) and model prediction..... 12

Figure 12. Plot of fluorescence intensity with changing NO concentration 13

Figure 13. Fluorescence intensity trace as NO concentration was changed from 0 to 0.247 ppm_v..... 14

1. Introduction

Laser-induced fluorescence has gone beyond its laboratory origins as a sensitive, selective method of detection of gas-phase molecules to find applications in several types of field measurements. Several of these applications involve the measurement of NO, in particular the areas of atmospheric chemistry, pollution monitoring, and combustion.[1–7] Our interest in NO detection came out of work on the detection of explosives.[8] NO fluorescence requires excitation in the ultraviolet, where typical laser sources are large and complex. Field applications require systems that are compact, robust, portable, low-power, inexpensive, and operable over a large range of ambient conditions. Passively Q-switched Nd:YAG/Cr^{4+}:YAG microchip lasers meet all of these requirements and provide all-solid-state sources of coherent, subnanosecond, multikilowatt pulses at high repetition rates.[9–15]

Prior to this report, all of the passively Q-switched Nd:YAG/Cr^{4+}:YAG microchip lasers had been operated at 1.064 μm or 946 nm. The harmonics of these sources do not overlap the NO absorption bands and are not useful for NO detection. It is possible to use a combination of parametric processes and harmonic conversion to get a useful wavelength,[12–17] but this results in a more complicated device with reduced power and wavelength stability. Nd:YAG has a gain peak at 1.074 μm, whose fifth harmonic, at 214.8 nm, falls within the NO absorption bands. A frequency-quintupled passively Q-switched Nd:YAG/Cr^{4+}:YAG microchip laser operating at this wavelength provides a compact, robust light source for the measurement of NO. The main challenge in building such a source is the close proximity of the dominant 1.064-μm gain peak, whose effective gain cross section is about twice as large.[18,22] In the microchip laser there are no intracavity frequency selective elements that can be used to discriminate between the two lines; all of the discrimination must be done with the laser mirror coatings. In field applications, the laser must operate over a range of temperatures and humidities, placing additional requirements on the coatings.

In the remainder of this report, we briefly discuss the operation of passively Q-switched microchip lasers and derive a set of coating requirements for a 1.074-μm device. We then discuss how we met these challenging requirements to produce an extremely robust 214.8-nm fifth-harmonic system capable of detecting NO at the few-ppb_v level. We report on laser characterization experiments using NO fluorescence excited by the 214.8-nm source, and compare with earlier observations of SO_2 fluorescence using a 212.8-nm microchip laser (fifth harmonic of 1.064 μm) and of NO_2 fluorescence excited by the 532-nm light of the same laser system.

2. Laser Development

2.1 Operating Principle

The principle behind the operation of a passively Q-switched laser is that an intracavity saturable absorber prevents the onset of lasing until the average inversion density within the cavity reaches a critical threshold value. The onset of lasing, at that point, produces a high intracavity optical field that saturates the saturable component of the optical loss, increasing the cavity Q and resulting in a Q-switched output pulse. In their simplest embodiment, the passively Q-switched microchip lasers developed at MIT Lincoln Laboratory are constructed by diffusion bonding a thin, flat wafer of Nd:YAG gain medium to a similar wafer of Cr^{4+}:YAG saturable absorber. The composite structure is polished flat and parallel on the two faces normal to the optic axis. Cavity mirrors are deposited directly onto the polished faces. The infrared laser is completed by dicing the wafer into small squares, typically 2 mm on a side. The YAG cavity is mounted on a heatsink and longitudinally pumped with a diode laser. The simplicity of the passively Q-switched microchip laser and its small amount of material give it the potential for inexpensive mass production; nearly monolithic construction results in robust devices.

A schematic of the 1.074-μm passively Q-switched microchip laser is shown in Fig. 1. The laser consists of 2 mm of undoped YAG, 1.5 mm of Nd:YAG, 0.6 mm of Cr^{4+}:YAG, and 2 mm of undoped YAG, diffusion bonded to each other in the order listed. The Nd:YAG is doped at 1.1 wt.% Nd. The Cr^{4+}:YAG has an unsaturated absorption coefficient of 6 cm^{-1} at both 1.064 and 1.074 μm. The undoped YAG endcaps are used to lengthen the output pulses and improve the damage threshold of the devices.[12–15] The input coating of the laser must be highly transmitting at the pump wavelength of 808 nm and highly reflecting at the oscillating wavelength. Since there are already dual wavelength requirements on this coating, we perform all of the discrimination against the 1.064-μm Nd transition with the output coating.

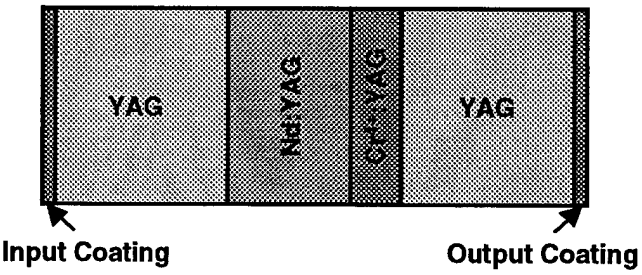

Figure 1. Schematic of a 1.074-μm passively Q-switched microchip laser.

The passively Q-switched microchip laser reaches threshold when the inversion density is sufficient to generate round-trip gain that is greater than the unsaturated round-trip loss. In the laser there are two main sources of loss, the intracavity loss due to the presence of the Cr^{4+}:YAG saturable absorber and the transmission of the output coupler. The round-trip loss of an optical beam within the (unsaturated) cavity is

$$L_\lambda = 1 - \exp(-2\alpha_\lambda l_\alpha) R_\lambda,$$

where α_λ and R_λ are the unsaturated absorption coefficient and reflectivity of the output coupler at wavelength λ, and l_α is the length of the saturable absorber. The gain of the active cavity is

$$G_\lambda = \exp(2n_{i\lambda}\sigma_\lambda l_g),$$

where $n_{i\lambda}$ and σ_λ are the inversion density and the effective gain cross section at wavelength λ, and l_g is the length of the gain medium. To obtain lasing at 1.074 μm, we must satisfy the condition

$$G_{1.074}(1-L_{1.074}) = 1.$$

To suppress lasing at 1.064 μm,

$$G_{1.064}(1-L_{1.064}) < 1.$$

Optimal performance of a passively Q-switched Nd:YAG/Cr^{4+}:YAG microchip laser is obtained for[19]

$$R_{1.074} \approx \exp(-\alpha_{1.074} l_\alpha).$$

Since, for Cr^{4+}:YAG, $\alpha_{1.064} \sim \alpha_{1.074}$ and $n_{i1.064} \sim n_{i1.074}$, suppression of oscillation at 1.064 μm requires

$$R_{1.064} < (R_{1.074})^\zeta,$$

where

$$\zeta = 3\left(\frac{\sigma_{1.064}}{\sigma_{1.074}}\right) - 2.$$

For Nd:YAG, $\sigma_{1.064} \sim 2\sigma_{1.074}$, requiring that $R_{1.064} < (R_{1.074})^4$.

2.2 Optical Coating

The optical coatings for the microchip laser were produced using an electron-beam evaporation system equipped with a single-rotation semi-spherical substrate holder and 6-kW quartz substrate heaters. The system has an ion-assisted-deposition (IAD) capability that uses a 5-A end-Hall ion source with typical ion energies of 80 – 120 eV.

The pump-side coating on the microchip laser has a nominal specification of <5% reflectivity at 808 nm and >99.9% reflectivity at 1.074 μm. The output coating is specified to have <5% reflectivity at 1.064 μm and 70±5% reflectivity at 1.074. These output coating specifications are somewhat more severe than the above derivation requires, reflecting a large uncertainty in the ratio of the emission cross sections at 1.064 and 1.074 μm.

For the input coating, we used our standard 21-layer edge-filter design, giving >99.9% reflectivity at both 1.064 and 1.074 μm and typically <1% reflectivity at 808 nm. The enhanced spectral stability associated with IAD techniques was not required for this coating, but the IAD process was used to give a higher damage threshold.

The output coupler used a 21-layer quarter-wave stack followed by a half-wave low-index layer. The design has a very steep skirt on the short-wavelength end of the high-reflectance band, as shown in Fig. 2, giving the required discrimination between the 1.074- and 1.064-μm lines (<1% reflectivity at 1.064 μm and 70% reflectivity at 1.074 μm, theoretical). This translates into a steepness of ~7%/nm. In order to achieve the ±5% reflectivity specification at 1.074 μm, the edge of the high-reflectance band must be positioned within 0.7 nm, or 0.07%, and remain there over the full range of environmental conditions encountered during the operation of the device.

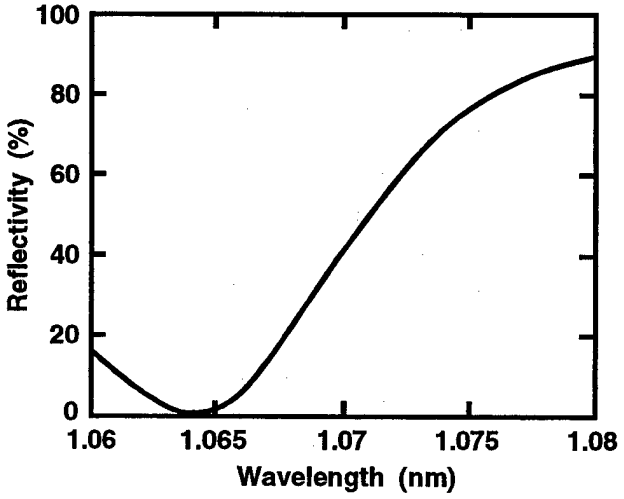

Figure 2. Theoretical reflectivity of output coupler.

To achieve the required environmental stability, electron-beam IAD was used in conjunction with an elevated substrate temperature (~200°C). The ion source was operated at 0.3 mA/cm^2 (4.5-A anode current) at 100 – 110 eV (150 – 160-V anode voltage). This results in a dense film morphology and low porosity to give the coatings a high degree of spectral stability. It also results in high-damage-threshold coatings, which we have used[12–15] on high-power microchip lasers with output intensities in excess of 10 GW/cm^2. We measured the spectral stability of these coatings to be better than ±0.05% immediately following exposure to a wide range of ambient conditions, including vacuum bake, exposure to 60% humidity for 5 days at room temperature, and immersion in boiling water.

The high accuracy required for the output-coupler coating was achieved by taking advantage of the thickness runoff that normally occurs along the radius of the rotating substrate holder. In-situ optical monitoring allows us to obtain 1% thickness accuracy at a given radial position. Thickness runoff over the radius of the substrate holder is much greater than this. If many substrates are mounted along the radius of the substrate holder, it is possible to adjust their spacing so that at least one has the desired coating properties.

Without any distribution shields, our optical coater has a nearly linear thickness runoff of ~0.6% per radial cm. With a 6.5-cm-wide shield extending radially across the substrate holder, the runoff was reduced to ±1% over a radial distance of 10 cm (see Fig. 3). Twelve 2 × 2-mm microchip lasers were positioned radially over this distance, guaranteeing that several of the devices would have coatings meeting the reflectivity specifications.

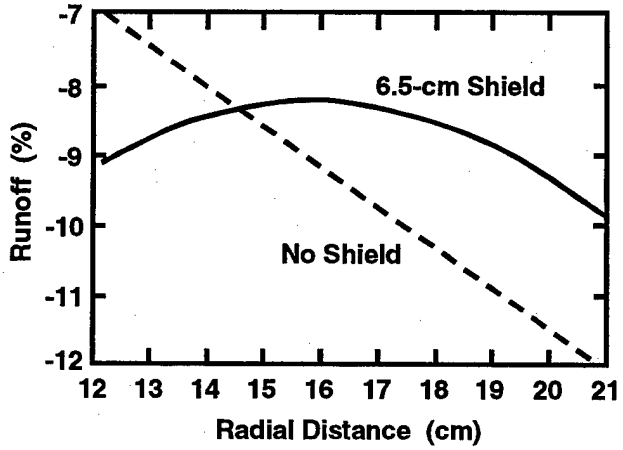

Figure 3. Spectral runoff of optical coater with and without 6.5-cm distribution shield.

After coating, the reflectivity of the output surface of each of the microchip lasers was measured at near-normal incidence using a 1.064-μm laser. The reflectivity of witness samples spanning the same radial distances was also measured at both 1.064 and 1.074 μm. The results are shown in Fig. 4, where the microchip lasers have been assigned numbers from 1 to 12, and

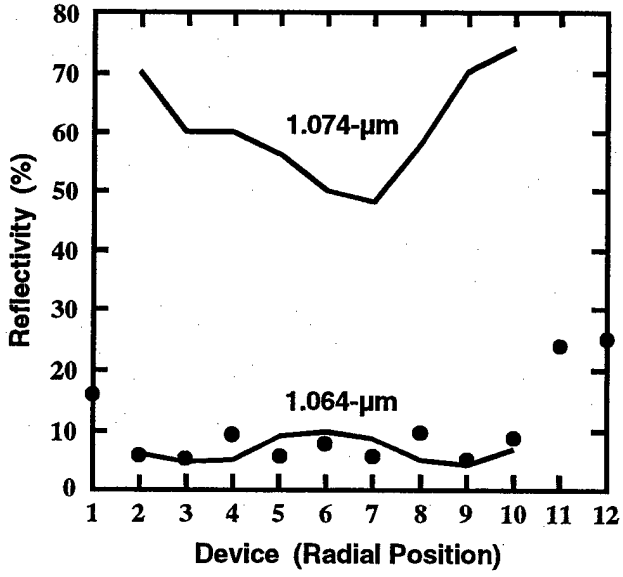

Figure 4. Spectral properties of output coatings on 12 microchip lasers (circles) and radially collocated witness samples (lines).

the measurements of the witness samples have been radially collocated with the microchip lasers. The measurements indicated that devices 2 – 4 and 8 – 10 should be closest to meeting the coating specifications.

The microchip lasers were longitudinally pumped with the fiber-coupled output of a 12-W diode-laser array. The pump-delivery fiber has a core diameter of 490 μm and a numerical aperture of 0.12. Its output was imaged into the Nd:YAG gain medium with a 0.25 magnification using a pair of aspheric lenses. Pumping was done in a quasi-cw fashion at 1-kHz repetition rate. Devices 3 and 7 failed due to coating damage; devices 2, 4, 5, and 10 were 1.074-μm lasers; the other devices operated at 1.064 μm. These results are in general agreement with the spectral measurements and our understanding of the coating requirements (some deviations between the coatings on the microchip lasers and the witness samples are expected).

2. 3 Device Operation

All of the 1.074-μm microchip lasers have similar properties. When pumped as described above, the minimum pump duration required for the passively *Q*-switched lasers to produce an output pulse is 120 μs. Each of these lasers can be operated at repetition rates up to 2 kHz, and produces an output pulse with a typical pulse energy of 30 μJ and duration of 1.6 ns, in a single longitudinal mode with a linearly polarized, 85-μm-radius ($1/e^2$ intensity), diffraction-limited transverse mode.

Device 4 was used to construct a 214.8-nm source. Its output is frequency converted with a set of antireflection-coated nonlinear crystals that was optimized for frequency conversion of a 1.064-μm laser.[10–15] All of the nonlinear crystals have flat, parallel faces and are butt coupled to each other (and the microchip laser) without any intervening optics. Second-harmonic generation is performed using Type II phase matching in a 5-mm-long piece of KTP, resulting in 8 μJ/pulse of 537-nm light. The slightly-lower-than-expected conversion efficiency is a result of the large angle between the incident light and the normal to the KTP surface (~14°, compared to 5° for frequency doubling of 1.064-μm radiation[13]), resulting in greater reflection losses than would be otherwise expected. The output of the KTP is frequency doubled in a 5-mm length of BBO using Type I phase matching. This produces 1.2 μJ/pulse of 268-nm light, which is frequency summed with the fundamental (1.074 μm) using Type I phase matching in a second 5-mm-long piece of BBO. The result is 50 nJ (±20%) of fifth-harmonic light at the desired 214.8-nm wavelength. The entire optical head (fiber-imaging optics, microchip laser, and nonlinear crystals) is packaged in a 1.5-cm-diameter × 8-cm-long stainless steel can, whose only input is the pump-delivery fiber (see Fig. 5).[12–15]

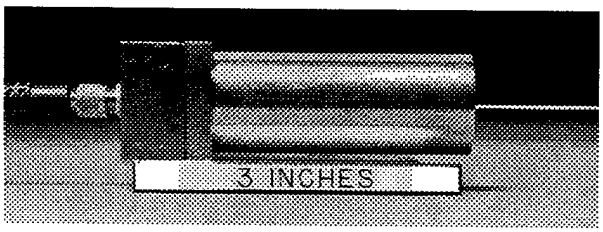

Figure 5. Photograph of optical head of fifth-harmonic 214.8-nm microchip laser source.

3. NO Fluorescence Observations

3.1 Experimental Setup

Figure 6 shows a schematic drawing of the apparatus used to determine the spectral position and detection sensitivity of the laser. The laser is mounted in a heat sink, and its output is passed through a Brewster-angle prism and an aperture to separate out the 214.8-nm beam. The fluorescence cell is a 1-cm-diameter, 15-cm-long quartz tube with integral Brewster-angle windows and inlet and outlet tubes to allow a flow of gas through the cell. A gas mixture containing 200 ppm_v NO is further diluted with air to make NO mixtures in the 0.2 to 5 ppm_v range. The flow rates and cell pressure can be set independently, and the cell pressure can be read using a mechanical gauge.

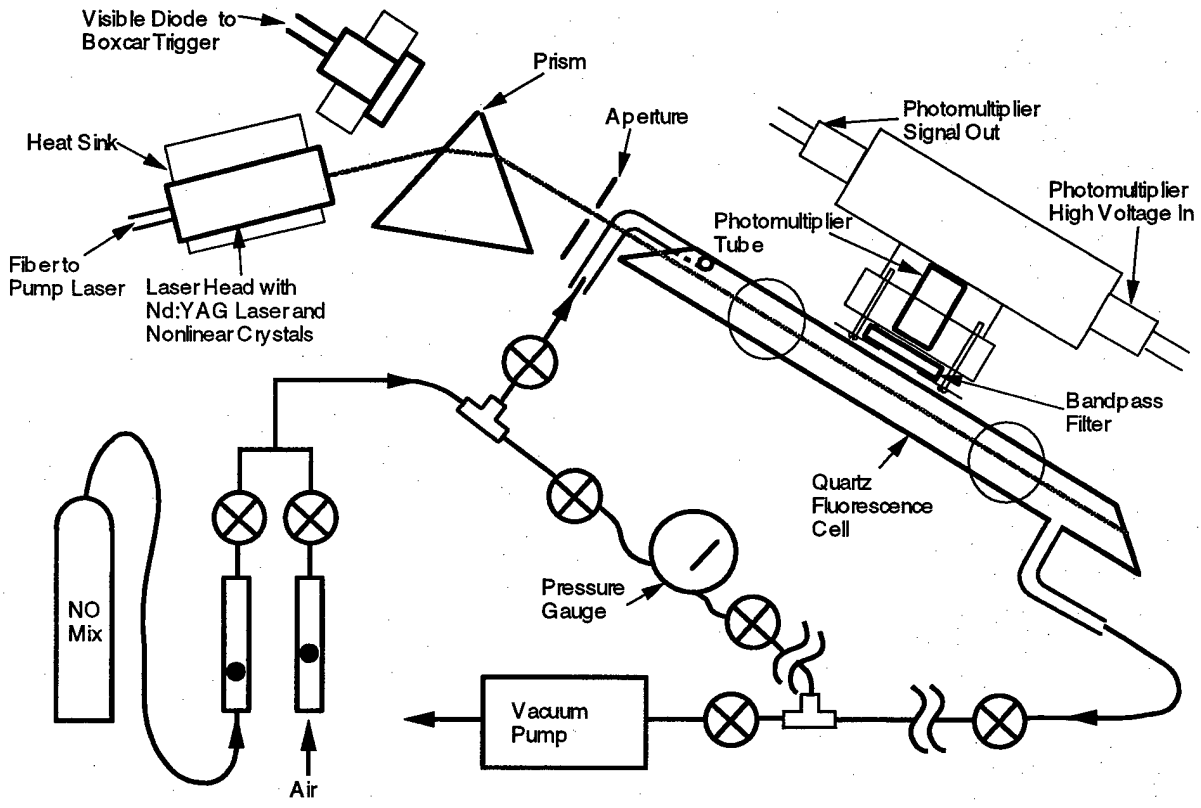

Figure 6. Schematic diagram of apparatus used in NO fluorescence observations.

The photomultiplier tube used was a Hamamatsu R5600U-03 with a bialkali photocathode with a nominal spectral response range of 185 to 650 nm. This tube is packaged in a TO-8 metal can, with length and diameter 1 cm and 1.5 cm, respectively. It mounts in a socket with only slightly larger dimensions, which contains a built-in voltage divider, resulting in a very compact detector assembly, as seen in the figure. The bandpass filter placed in front of the photomultiplier tube was an Oriel 51122, with a peak transmission of 89% and half-power points

at 245 and 390 nm. Its transmission at 214.8 nm is about 10^{-5} of the peak value. The relationship of the filter bandpass and the fluorescence emission spectrum is shown in Figure 7. In this figure, the laser line at 214.8 nm is shown at the far left. It excites transitions in the (1,0) band of the NO γ (A←X) system. Each excited state emits in a number of lines, whose relative intensities are determined in part by Franck-Condon overlaps and in part by relative rates of collisional quenching and energy transfer. In Figure 7, only the Franck-Condon factors are used to indicate approximate intensities. Since the first excited vibrational state (v'=1) in the upper electronic state is populated by the laser excitation, we expect v'=1 and v'=0 states to contribute the most to the emission spectrum.

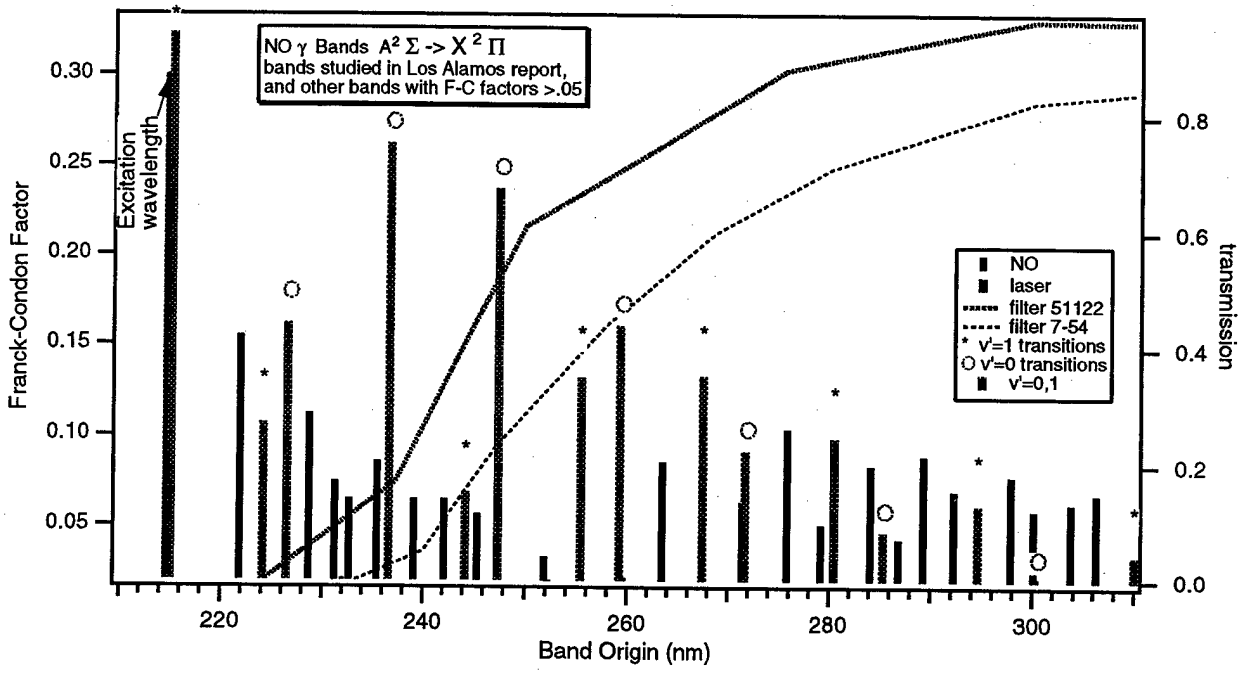

Figure 7. Filter bandpass curves (Oriel 51122 was used in experiments discussed here) and spectral locations and relative intensities of fluorescent emission lines (see Ref. 24).

3.2 Spectral Position

A key to understanding the detection capabilities of devices using this laser is an accurate knowledge of its frequency, and in particular of the fifth-harmonic line position relative to NO spectral line positions. The level of uncertainty at the beginning of our investigation is illustrated by the values in four standard reference works: Danielmeyer[18], Pressley[20] (who quotes a value due to Smith[21]), and Kaminskii[22] and Koechner[23] (who consider 10 and 4 primary references, respectively). When translated into fifth harmonic frequencies, the four fundamental wavelengths quoted yield values of 46559.3, 46569.7, 46567.9, and 46563.6 cm^{-1}. Kaminskii also lists a linewidth (of the fundamental) of 7 cm^{-1}, or a range of possible fifth-harmonic

frequencies of 35 cm^{-1}, larger than the spread in quoted center positions of a little over 10 cm^{-1}. Furthermore, all of the above values are for crystals nominally at room temperature. We expect the crystal in our device to be at an elevated temperature, about 10°C above room temperature. Danielmeyer quotes a decrease in transition energy with increasing temperature of 0.04 cm^{-1}/°C. This could correspond to a 2-cm^{-1} decrease in fifth-harmonic frequency for our expected crystal temperature. With this level of uncertainty, a positive determination of the laser fifth-harmonic frequency was clearly of interest.

Our approach was to temperature-tune the laser fundamental by changing the pump laser repetition rate, thus generating excitation spectra with an unknown frequency scale. Our only constraint was that we expected our tuning range to be on the order of the free spectral range of the laser cavity, 13.5 GHz (0.45 cm^{-1}) at the fundamental, 67 GHz (2.25 cm^{-1}) at the fifth harmonic. Because the fractional changes in repetition rate were small (from about 800 to 1200 Hz) the temperature changes were also small and we expected a linear relationship between repetition rate and laser frequency. The frequency scale was set by comparison to the predictions of a model of the spectrum. Three types of parameters had to match: line-frequency separations, line widths, and relative line intensities. It turned out that only one set of NO features matched within the spectral range considered, leading to a positive identification of the fifth-harmonic frequency under our operating conditions, 46556 cm^{-1}.

3.3 Spectral Model

In our model, the NO line positions were taken from the experimental observations of Engleman et al.,[24] supplemented by values reported by Gero and Schmid[25] for bands not reported by Engleman et al. Examples of comparisons with two further data sets, not including the band of interest here, are presented by Engleman et al., who cite the average differences of 0.00 ± 0.33 and 0.01 ± 0.10 cm^{-1} as support for their claim that their line measurements are good to 0.01 cm^{-1} or better. On the other hand, comparison between Engleman et al. and Gero and Schmid values also shows many differences at the few-tenths-of-a-wavenumber level. Since such comparisons do not show how much of the deviation resides with each measurement, we have to consider our model line positions to be uncertain by at least 0.1 cm^{-1}.

The model line strengths S in cm^{-1} $(molecule/cm^2)^{-1}$ were estimated using the expression

$$S = (n_e/n)(n_J/n)\, S_J\, (q_{vv}/\tau)/(8\pi c\nu^2) .$$

In this equation, the electronic-state population fraction (n_e/n) is derived from the Boltzmann factors for a two-level system with the energy separation of the $^2\Pi_{3/2}$ and $^2\Pi_{1/2}$ states. The rotational-state population fraction (n_J/n) is the ratio of $(2J+1)\exp(-E_J/RT)$ to its sum, where the rotational energy E_J was calculated using the expressions given by Dodge et al.[26] The Hönl-London factors S_J have been worked out by Earls.[27] The Franck-Condon factor q_{vv} is 0.33 and the radiative lifetime τ is taken as 1.9×10^{-7} s. Finally, ν is the transition frequency in wavenumbers. Combining all factors not dependent on the individual line quantum numbers,

$$S = 2.3 \times 10^{-6}\, (n_e/n)(n_J/n)\, S_J/\nu^2 .$$

In addition to line strength and frequency, the third parameter needed for a spectral model is the pressure-broadened line width. From the measurements reported by Dodge et al.[26] and Chang et al.[28] for lines other than those of interest here, we chose a line width coefficient (half width at half maximum) of 0.55 cm^{-1}/atm. We used the model to predict the NO absorption coefficient from 46540 to 46600 cm^{-1}. Although a number of additional factors are needed to predict fluorescence intensity, over this restricted spectral region none of them is frequency dependent, and we can match the shape of the observed fluorescence spectrum to the various candidate features in the predicted absorption spectrum.

3.4 Comparisons of Model and Observed Excitation Spectra

The result of this procedure is shown in Figure 8. Two experimental spectra, shown in dots and dashes, are compared with a model spectrum (solid line). The observations shown by the dots were made by changing the pump laser repetition rate by 10 Hz once a minute, allowing the laser temperature to stabilize after each discrete change. The dashed line was obtained by changing the repetition rate by 1 Hz every 6 s, thus generating a continuous chart paper record which was later digitized.

Spectra obtained at a reduced pressure, 122 Torr, were considered first for several reasons. The narrower lines make it easier to determine peak frequencies, the fact that the Doppler width is almost as large as the pressure-broadened width reduces the uncertainty in this model parameter, and the low pressure makes it easier to see smaller neighboring lines. The NO spectrum throughout the region studied consists largely of pairs of lines like those shown in Figure 8. However, many have shoulders or small nearby lines which would easily distinguish them, and those few that are isolated pairs have different intensity ratios, so that the spectral region in Figure 8 is the only one which gives a good match to our observations.

Returning to the question of the accuracy of the line positions in the model, the frequencies shown are those of Engleman et al., with $R_1(3)$ and $Q_1(10)$ lines at 46555.305 and 46556.668 cm^{-1}, while Gero and Schmid report frequencies of 46554.97 and 46556.44 cm^{-1}. Therefore, the line spacing shown in the figure is 1.363 cm^{-1}, while the line spacing using the values of Gero and Schmid would be 1.47 cm^{-1}, or 8% larger. It can be seen that if the line widths were allowed to set the frequency scale rather than the line separation, we would conclude that the observed line pair was actually spaced by more than 1.5 cm^{-1}. However, our repetitions of spectral scans show us that variations in laser-crystal temperature can lead to at least 10% uncertainties in experimental line widths and peak separations. Therefore, the level of agreement between model and experiment is more than adequate to convince us that we have the correct assignment for the observed lines.

We also made observations of the same two lines at three more pressures, 240, 480 and 740 Torr. These spectra are shown in Figures 9–11. The expected broadening of the lines with increasing pressure is observed, along with some experimental artifacts in the tuning rate, as mentioned above.

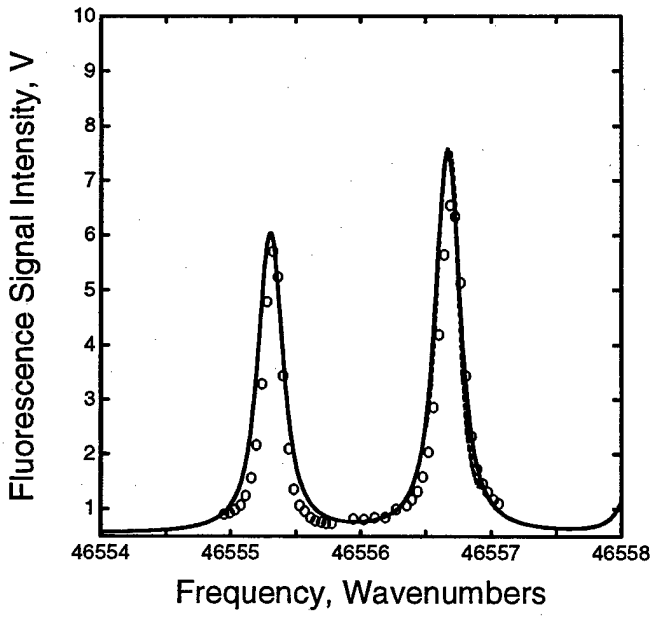

Figure 8. Observed fluorescence excitation spectrum at 122 Torr (dots/dashes) and model prediction.

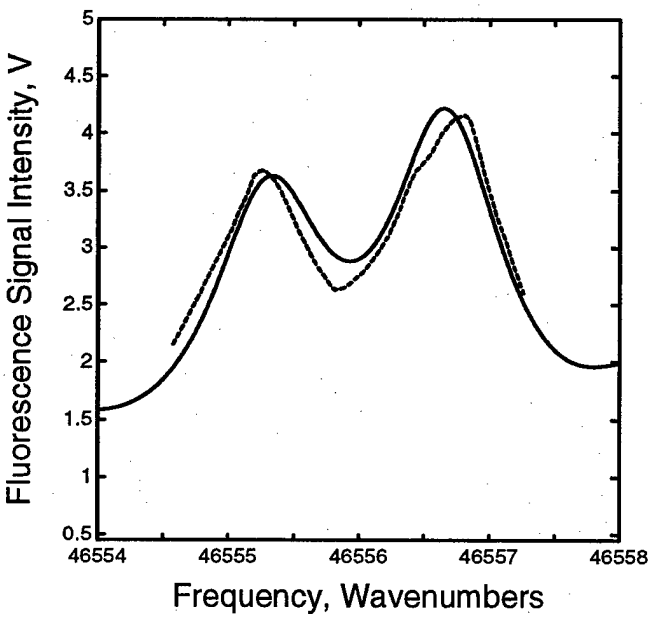

Figure 9. Observed fluorescence excitation spectrum at 740 Torr (dashes) and model prediction.

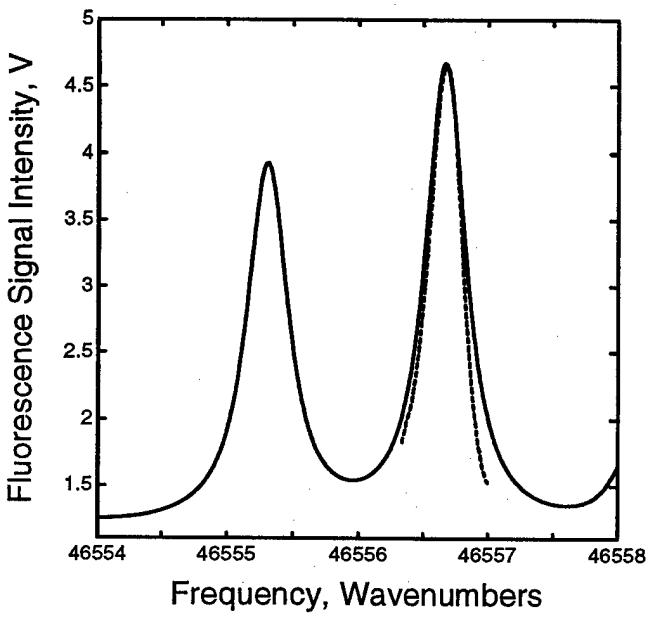

Figure 10. Observed fluorescence excitation spectrum at 240 Torr (dashes) and model prediction.

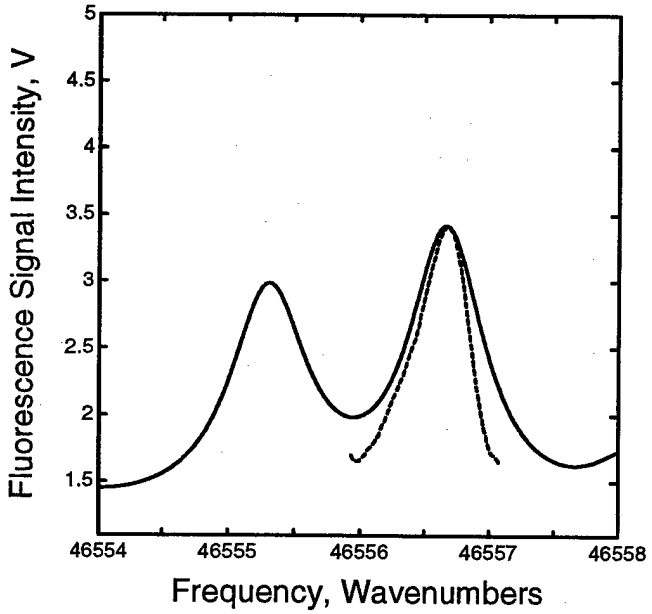

Figure 11. Observed fluorescence excitation spectrum at 480 Torr (dashes) and model prediction.

3.5 Calibration and Detection Linearity

NO fluorescence intensity should respond linearly to changes in NO concentration (at low NO levels). The fact that we observe the linear behavior shown in Figure 12 indicates the absence of experimental artifacts which might interfere with the derivation of an ultimate detection sensitivity for the system. An unconstrained linear fit through the points yields zero fluorescence intensity at an NO concentration of -0.03 ppm_v. The scattered light level was measured separately and subtracted from all points. By the time the spectra in Figures 8–11 were taken, the scattered light level was about 0.1 of the peak signal level with the fluorescence cell at 1 atm, although the ratio of fluorescence signal to scattered light was somewhat higher in the earlier measurements used for Figure 12.

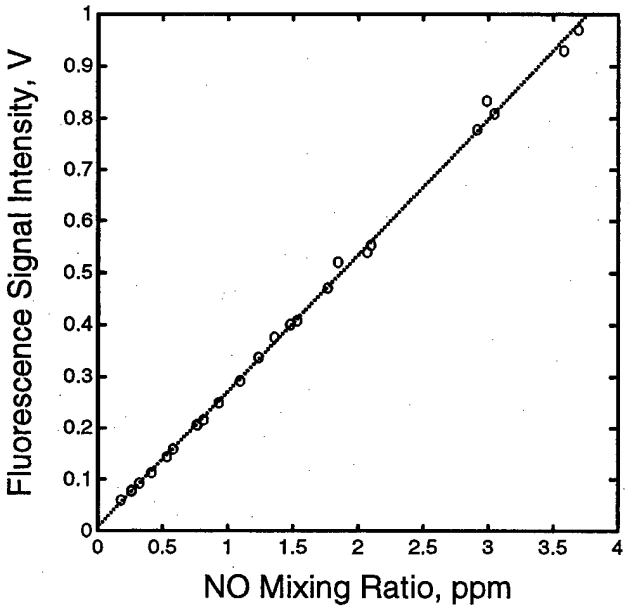

Figure 12. Plot of fluorescence intensity with changing NO concentration.

3.6 Detection Sensitivity

Figure 13 shows the implications of the current system noise level for its ultimate detection sensitivity. On the left is the photomultiplier signal due to scattered light only, and on the right is the signal after NO has been added to the flow through the cell. The linear calibration from Figure 12 has been used to set the vertical scale, while the NO concentration derived from flowmeter readings was 0.247 ppm_v. The boxcar averaging was set to give a 1-s time constant. Under these conditions, the standard deviation in fluorescence signal corresponds to an NO concentration of 15 ppb_v. Application of fluorescence intensity estimates[29,30] allows us to conclude that this corresponds to a signal level on the order of one fluorescence photon per

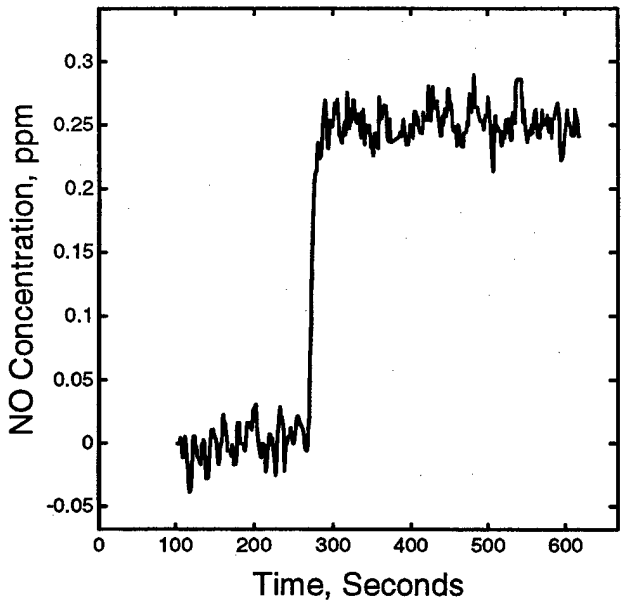

Figure 13. Fluorescence intensity trace as NO concentration was changed from 0 to 0.247 ppm_v.

pulse. It turns out that the noise spectrum of the trace in Figure 13 is such that a 1 minute average only reduces the standard deviation by a factor of two.

In some applications, the measurement will proceed as indicated in Figure 13: gas containing NO at some baseline concentration will be sampled and the corresponding level of fluorescence will be established, then gas containing a higher level of NO will be admitted into the fluorescence cell and the difference between the two levels will be used to derived the change in concentration. Under these circumstances, the standard deviation is directly related to the detection sensitivity. In other applications, where quantification of an absolute level rather than detection of a sudden change are of interest, the sensitivity of the system may depend on long term drifts as well as short term noise.

The detection sensitivity using this laser is, of course, also highly dependent on other characteristics of the system. Our analysis of noise levels yields some unremarkable conclusions: at low concentrations, contributions from photomultiplier dark current and other sources of noise observable with the laser blocked are comparable to contributions from fluctuations in scattered light, and as fluorescence light is added to these signals, the increase in noise follows the square root of the number of fluorescence photons. This means that some additional gains in detection sensitivity can be made, for example by further decreasing scattered light, and that higher laser power delivered into the fluorescence cell will decrease the minimum detectable concentration. However, these can be expected to be relatively modest improvements. In high sensitivity detection systems described in the literature, the largest gains over the system reported here come from using multiple passes of the excitation beam, and from averaging for much longer times than the 1 s used in our data acquisition.

4. SO_2 and NO_2 Observations with Microchip Lasers

One of the particularly attractive potential applications of the microchip lasers studied here is a system which uses the fifth and second harmonic beams to make laser induced fluorescence measurements of NO and NO_2, respectively. Another application we hope to pursue is the use of the fifth harmonic to detect SO_2. The absorption lines of SO_2 and NO_2 are closer together than those of NO, so that at atmospheric pressure the laser wavelength is much less critical and the harmonics of either a 1.064- or 1.074-μm laser can be used to make laser induced fluorescence measurements. Therefore, we used these gases in conjunction with a 1.064-μm microchip laser to study detection sensitivity issues while the 1.074-μm laser was being constructed. Preliminary results for SO_2 and NO_2 were presented in our first annual report for this Phase 2 project,[29] and in our Phase I final report,[30] respectively. Here, we briefly review additional measurements and their relationship to the NO observations already described.

4.1 SO_2 Laser-Induced Fluorescence

Using a 212.8-nm laser (fifth harmonic of 1.064 μm) we performed SO_2 detection-sensitivity measurements analogous to those documented for NO in Figures 11 and 12. Considering differences in quenching rates and absorption coefficients, we estimated that the SO_2 detection limit at either 212.8 or 214.8 nm would be 2.4 times lower (more sensitive) than that for NO, for the same laser power and detection parameters. On the other hand, we estimated the power of the laser used in the SO_2 experiments to be about 3 nJ/pulse, compared to the 50 nJ/pulse for the NO laser, although the SO_2 laser was operated at 10 kHz rather than 1 kHz for the NO laser. In our observations, we found that the standard deviation of the scattered light signal corresponded to a SO_2 concentration of about 150 ppb_v. This higher noise level comes from a larger fractional standard deviation due to the lower laser power level: the ratio of standard deviation to fluorescence signal for 4 ppm_v NO is about 0.0015, while that for our SO_2 observations with the lower power laser was about 0.08. This difference in noise level is partially compensated by greater sensitivity to SO_2, resulting in the order-of-magnitude difference in the two concentration detection limits. It is clear that the higher-power laser should result in SO_2 detection limits comparable to those observed for NO.

4.2 NO_2 Laser-Induced Fluorescence

Once again, detection sensitivity measurements like those of Figure 12 for NO were performed for NO_2. We first made observations, using a Hamamatsu R955 photomultiplier tube because the fluorescence peaks around 700 nm, which differed from those presented in Reference 30 only in that the optical layout was confined inside a box with width, depth and height of 12, 7 and 3 inches. Our goal in transferring the setup to this box was to take the first step in engineering compact sensing devices to take advantage of the distinctive properties of the microchip laser. The resulting sensitivity plot was similar to the earlier observations presented in Reference 30. The key point in both data sets is the lower sensitivity to NO_2 using laser induced fluorescence pumped by green light, in comparison to the ultraviolet-pumped fluorescence sensitivities discussed above.

Our most recent NO_2 studies, carried out just after the SO_2 observations described in the preceding section, showed fluorescence intensities almost 500 times lower than those for the same concentrations of NO. We expect this, with the differences in absorption coefficient and in fraction of fluorescence which is quenched, as outlined in Reference 30, being the key factors. Specifically, the ratio of fluorescence emission rate to quenching rate is over 200 times lower for NO_2 than for NO, while the NO_2 absorption cross section is over 40 times lower than the peak NO value. These factors more than overcome the larger laser intensity at 532 nm, which for these observations was about 2 μJ/pulse or about 40 times the 50 nJ/pulse in our NO experiments. Other parameters with differences include the filter transmission, the collection solid angle, and the photomultiplier sensitivity and amplification, but these are all changes of factors of two or less. The result of calculations along the lines of those presented in Reference 30 is that the ratios of fluorescence intensity in our NO and NO_2 observations are just what should be expected based on the differences in molecular parameters and detection-system properties.

We noted above that fluorescence-intensity estimates allow us to interpret the 15-ppb_v detection limit for NO as a signal level on the order of one fluorescence photon per pulse. If one photon per pulse were also the noise-equivalent signal level for NO_2 detection, this would correspond to an NO_2 concentration of a bit under 1 ppm_v. We expect very similar detection levels for the NO-capable laser, since its 537-nm energy was 7 μJ/pulse or about 4 times the 532-nm pulse energy used in the study described above, while the NO_2 absorption cross section at 537 nm is about a factor of two lower than that at 532 nm.

One additional aspect to our NO_2 studies was the evaluation of a Hamamatsu R5600U-01 photomultiplier tube, with the same highly compact design as the R5600U-03 we used for our NO observations. We found it was significantly less sensitive than the conventional Hamamatsu R955 we used in our earlier observations, by almost a factor of 30, and so would result in a much less useful instrument. We expect, however, that if the demand were demonstrated, compact photomultiplier tubes with good sensitivity in the NO_2 fluorescence spectral range (centered at 700 nm) could be developed.

5. Discussion and Conclusions

The key achievement presented in this report is the development and characterization of a microchip-laser system delivering the fifth harmonic of the 1.074-μm Nd:YAG fundamental line. Analysis of NO fluorescence spectra covering a range of almost 3 cm^{-1} identified the fifth-harmonic nominal frequency as 46556 cm^{-1}. This is an excellent position for sensitive and selective detection, since it lies between two strong NO absorption lines, with either peak being easily accessed by temperature tuning the laser.

We demonstrated detection levels for NO in the few-ppb_v range, in a system by no means optimized for ultimate detection sensitivity. Detection of SO_2 with similar sensitivity was also demonstrated, while the second-harmonic (green) output of these microchip lasers can be used for simultaneous detection of NO_2 at sub-ppm_v levels. Avenues for further development include increases in sensitivity, based on a careful analysis of the noise sources discussed in this report, and the engineering of the laser and detection system into smaller and more rugged packages for field measurement applications.

The system we studied lies between two limiting types of interesting systems. On the one hand are systems optimized for high-sensitivity detection, quite possibly with additional size, weight, and expense compared to the one described here. As mentioned above, extremely high sensitivity devices for measuring trace concentrations in the atmosphere employ such techniques as multipass excitation, long-time averaging, and elaborate means of suppressing scattered excitation light.[7,31–33] These modifications would increase the size, complexity, and response time of the system. On the other hand, we expect the compact size of the current laser will lead to applications in which the detection system is reduced in size from the layout we studied. This could result in useful systems with noise levels higher than those we report here.

There are several applications in which the microchip-laser system could offer real advantages. One is a generalization of the original motivation for our work: measurement of NO (and NO_2) in explosives detection systems, including contaminated site screening and security screening. A second area is measurement of both NO_x and SO_x in pollution-related studies, such as instrumentation of trucks or aircraft engines, and monitoring of stationary sources. Although other techniques are currently in use in these areas, microchip lasers offer a unique combination of small size, rugged construction, freedom from reagent chemicals such as ozone, and the sensitivity and selectivity characteristic of high-resolution laser spectroscopic techniques.

6. Acknowledgements

The authors gratefully acknowledge J. Daneu (MIT Lincoln Laboratory) for polishing and assembly of the optical crystals, A. Wilson (MIT Lincoln Laboratory) for help in the assembly and characterization of the 214.8-nm optical head, and M. S. Zahniser, D. D. Nelson, J. B. McManus, C. E. Kolb and P. L. Kebabian (Aerodyne Research) for helpful advice.

7. List of Publications and Technical Reports

A modified version of this report will be submitted to the journal Applied Optics. The only previous report submitted under this contract is the first annual report.[29]

8. List of All Participating Scientific Personnel

Participating scientific personnel included J. H. Shorter and J. Wormhoudt at Aerodyne Research and J. J. Zayhowski, C. Cook, B. Johnson and N. Newbury at MIT Lincoln Laboratory. No degrees were awarded as part of the work on the program.

9. Report of Inventions

No inventions were made under this program.

10. Bibliography

1. C. E. Kolb, "Instrumentation for chemical species measurements in the troposphere and stratosphere," Reviews of Geophysics Supplement , pp. 25–36 (1991).

2. H. I. Schiff, "Ground based measurements of atmospheric gases by spectroscopic methods," Berichte der Bunsengesellschaft **96**, 296–306 (1992).

3. J. Bublitz, M. Dickenhausen, M. Grätz, S. Todt and W. Schade, "Fiber-optic laser-induced fluorescence probe for the detection of environmental pollutants," Appl. Opt. **34**, 3223– 3233 (1995).

4. C. Schulz, V. Sick, J. Heinze and W. Stricker, "Laser-induced-fluorescence detection of nitric oxide in high-pressure flames with A-X (0,2) excitation," Appl. Opt. **36**, 3227–3232 (1997).

5. A. V. Mokhov, H. B. Levinsky and C. E. van der Meij, "Temperature dependence of laser-induced fluorescence of nitric oxide in laminar premixed atmospheric-pressure flames," Appl. Opt. **36**, 3233–3243 (1997).

6. B. E. Battles and R. K. Hanson, "Laser-induced fluorescence measurements of NO and OH mole fraction in fuel-lean, high pressure (1–10 atm) methane flames: fluorescence modeling and experimental validation," J. Quant. Spectrosc. Radiat. Transfer **54**, 521-537 (1995).

7. S. Sandholm, S. Smyth, R. Bai and J. Bradshaw, "Recent and future improvements in two-photon laser-induced fluorescence NO measurement capabilities," J. Geophys. Res. **102,** 28651–28661 (1997).

8. J. Wormhoudt, J. H. Shorter, J. B. McManus, P. L. Kebabian, M. S. Zahniser, W. M. Davis, E. R. Cespedes and C. E. Kolb, "Tunable infrared laser detection of pyrolysis products of explosives in soils," Appl. Opt. **35**, 3992–3997 (1996).

9. J. J. Zayhowski and C. Dill III, "Diode-pumped passively *Q*-switched picosecond microchip lasers," Opt. Lett. **19**, 1427–1429 (1994).

10. J. J. Zayhowski, "Microchip lasers create light in small places," Laser Focus World **32** (Penwell Publishing Co., Tulsa, Oklahoma), 73–78, April 1996.

11. J. J. Zayhowski, "Ultraviolet generation with passively *Q*-switched microchip lasers," Opt. Lett. **21**, 588–590 (1996); errata, **21**, 1618 (1996).

12. J. J. Zayhowski, "Passively *Q*-switched microchip lasers and applications," Rev. Laser Eng. **26**, 841–846 (1998).

13. J. J. Zayhowski, C. Dill III, C. Cook and J. L. Daneu, "Mid- and high-power passively *Q*-switched microchip lasers," in *OSA Trends in Optics and Photonics on Advanced Solid State Lasers,* M. M. Fejer, U. Keller, and H. Injeyan, eds. (Optical Society of America, Washington DC, 1999), pp. 178–186.

14. J. J. Zayhowski, "Passively *Q*-switched microchip lasers find real-world applications," Laser Focus World **35** (Penwell Publishing Co., Tulsa, Oklahoma), August 1999, to be published.

15. J. J. Zayhowski, "Passively *Q*-switched Nd:YAG microchip lasers and applications," Journal of Alloys and Compounds, 1999, to be published.

16. J. J. Zayhowski, "Microchip optical parametric oscillators," IEEE Photon. Tech. Lett. **9**, 925–927 (1997).

17. J. J. Zayhowski, "Periodically poled lithium niobate optical parametric amplifiers pumped by high-power passively *Q*-switched microchip lasers," Opt. Lett. **22**, 169–171 (1997).

18. H. G. Danielmeyer, "Progress in Nd:YAG Lasers," in *Lasers*, Vol. 4, A. K. Levine and A. J. DeMaria, eds. (Marcel Dekker, New York, 1976).

19. J. J. Degnan and J. J. Zayhowski, "SLR2000 microlaser performance: theory vs. experiment," *Proceedings of the 11th International Laser Ranging Workshop*, 1999, to be published.

20. R. J. Pressley, ed., *CRC Handbook of Lasers*, (Chemical Rubber Co., Cleveland, OH, 1971), p. 389.

21. R. G. Smith, "New room temperature CW laser transitions in YalG:Nd," IEEE J. Quantum Electronics, **QE-4**, 505–506 (1968).

22. A. A. Kaminskii, *Laser Crystals, Their Physics and Properties*, 2nd Ed. (Springer-Verlag, Berlin, 1990), p.242.

23. W. Koechner, *Solid-State Laser Engineering*, 2nd Ed. (Springer-Verlag, Berlin, 1988), p.53.

24. R. Engleman, Jr., P. E. Rouse, H. M. Peek and V. D. Balamonte, *Beta and Gamma Band Systems of Nitric Oxide*, Report LA-4364/UC-34, Physics/TID-44500, (Los Alamos Scientific Laboratory, Los Alamos, NM, 1970).

25. L. Gerö and R. Schmid, "Dissociation energy of the NO molecule," Proc, Phys. Soc. **60**, 533–540 (1948).

26. L. G. Dodge, M. B. Colket, III, M. F. Zabielski, J. Dusek and D. J. Seery, *Nitric Oxide Measurement Study: Optical Calibration*, Federal Aviation Administration Report FAA-EE-80-28, October, 1979, available Defense Technical Information Center, ADA109869.

27. L. T. Earls, "Intensities in $^2\Pi$– $^2\Sigma$ transitions in diatomic molecules," Phys. Rev. **48**, 423–424 (1935).

28. A. Y. Chang, M. D. DiRosa and R. K. Hanson, "Temperature dependence of collision broadening and shift in the NO A←X (0,0) band in the presence of argon and nitrogen," J. Quant. Spectrosc. Radiat. Transfer **47**, 375–390 (1992).

29. J. H. Shorter, J. Wormhoudt, C. E. Kolb, J. J. Zayhowski, B. Johnson, and N. Newbury, "Diode-pumped solid state laser based sensors for cone penetrometer applications," Aerodyne Res. Rep. ARI-RR-1233 (Aerodyne Research, Billerica, MA, December 1997).

30. J. H. Shorter, J. Wormhoudt, C. E. Kolb, J. J. Zayhowski, B. Johnson, and N. Newbury, "Diode-pumped solid state laser based sensors for cone penetrometer applications," Aerodyne Res. Rep. ARI-RR-1198 (Aerodyne Research, Billerica, MA, January 1997).

31. C. Fong and W. Brune, "A laser induced fluorescence instrument for measuring tropospheric NO_2," Rev. Sci. Instrum. **68,** 4253–4262 (1997).

32. P. S. Stevens, J. H. Mather and W. H. Brune, "Measurement of tropospheric OH and HO_2 by laser-induced fluorescence at low pressure," J. Geophys. Res. **99,** 3543–3557 (1994).

33. P. S. Stevens, J. H. Mather, W. H. Brune, F. Eisele, D. Tanner, A. Jefferson, C. Cantrell, R. Shetter, S. Sewall, A. Fried, B. Henry, E. Williams, K. Baumann, P. Goldan and W. Kuster, "HO_2/OH and RO_2/HO_2 ratios during the Tropospheric OH Photochemistry Experiment: Measurement and theory," J. Geophys. Res. **102,** 6379–6391 (1997).

REPORT DOCUMENTATION PAGE

Form Approved
OMB NO. 0704-0188

1. AGENCY USE ONLY *(Leave blank)*	2. REPORT DATE	3. REPORT TYPE AND DATES COVERED
	30 Jul '99	Final 1 Nov 96 - 30 Apr 99

4. TITLE AND SUBTITLE

Diode-Pumped Nd:YAG/Cr^{4+}:YAG Microchip-Laser System at 214.8 nm for the Detection of NO

5. FUNDING NUMBERS

DAAG55-97-C-0001

6. AUTHOR(S)

J. Wormhoudt, J.H. Shorter, J.J. Zayhowski, and C. Cook

7. PERFORMING ORGANIZATION NAMES(S) AND ADDRESS(ES)

Aerodyne Research, Inc.
45 Manning Road
Billerica, MA 01821-3976

8. PERFORMING ORGANIZATION REPORT NUMBER

ARI-RR-1282

9. SPONSORING / MONITORING AGENCY NAME(S) AND ADDRESS(ES)

U.S. Army Research Office
P.O. Box 12211
Research Triangle Park, NC 27709-2211

10. SPONSORING / MONITORING AGENCY REPORT NUMBER

ARO 36327.1-RT-ST2

11. SUPPLEMENTARY NOTES

The views, opinions and/or findings contained in this report are those of the author(s) and should not be construed as an official Department of the Army position, policy or decision, unless so designated by other documentation.

12a. DISTRIBUTION / AVAILABILITY STATEMENT

Approved for public release; distribution unlimited.

12 b. DISTRIBUTION CODE

13. ABSTRACT *(Maximum 200 words)*

A passively *Q*-switched 214.8-nm Nd:YAG/Cr^{4+}:YAG microchip-laser system for the detection of NO was designed, constructed, and tested. The system uses the fifth harmonic of the 1.074-μm transition in Nd:YAG to detect NO at the few-parts-per-billion level. A significant challenge was the development of an environmentally stable coating to provide the necessary discrimination between the 1.074-μm laser line and the stronger transition at 1.064 μm. The exact position of the fifth-harmonic frequency was determined using NO fluorescence excitation spectra to be 46556 cm^{-1}. We observed a detection sensitivity for NO of about 15 ppb_v in a simple, compact optical system. Earlier observations of SO_2 imply a similar or better sensitivity for the current system, while green-light excitation of NO_2 fluorescence yielded a detection limit of order 1 ppm_v. Applications of the laser system described here include explosives sensors based on detection of NO from thermal decomposition, and NO_x/SO_x monitors for trucks, aircraft and stationary sources.

14. SUBJECT TERMS	15. NUMBER IF PAGES
ultraviolet microchip laser, nitric oxide, sulfur dioxide, fluorescence detection	20
	16. PRICE CODE

17. SECURITY CLASSIFICATION OR REPORT	18. SECURITY CLASSIFICATION OF THIS PAGE	19. SECURITY CLASSIFICATION OF ABSTRACT	20. LIMITATION OF ABSTRACT
UNCLASSIFIED	UNCLASSIFIED	UNCLASSIFIED	UL